

Mathematical modeling of the impact of vehicles on water-saturated soil

Highlights

- A method has been developed to assess the impact of a wheel on waterlogged forest soil.
- The form of the transverse loading diagram has a significant effect on the degree of the stress state of the soil.
- Tires with reduced internal air pressure have the least impact on the ground.
- An application has been developed to assess the degree of soil compaction and the intensity of rutting during the operation of a forest machine.

Abstract

The presented mathematical model, together with its software implementation, makes it possible to assess the degree of influence of a vehicle on waterlogged forest soil, depending on the design parameters of the tire and the vertical loads on it.

The adequacy of the mathematical model is confirmed by the conducted experimental studies, as well as by numerous test results of forest machines.

The model is developed based on the theory of soil mechanics. The plane problem of compaction of water-saturated anisotropic (in the general case) soil is considered. It was shown that with an instantaneous application of a vertical load, the initial distribution of stress and water pressure in the soil are expressed through their values in a state of complete stabilization. Therefore, it is

20 conventionally assumed that the magnitude of the load does not change before the onset of this state,
21 causing linear (relative to the load) deformations of the soil.

22 Thus, first, a plane problem of different modulus of the theory of a linearly deformable medium is
23 solved. This problem is described by a system of partial differential equations. The solution is found by
24 the finite element method with respect to displacements. Then, the steady-state and initial values of the
25 stresses are determined, as well as the values of the maximum deviation of the total stress vector.

26 In the case of an isotropic medium, the initial fluid head function (H_o) satisfies the Laplace equation:
27 $\Delta H_o = 0$. The first boundary value problem is posed and solved. Analytical expressions are
28 obtained for the initial values of heads and stresses. With their help, one can select the optimal
29 triangulation of the region for a given loading diagram and check the finite element solution.

30 The calculation results are presented as level lines of a function of two variables. The general view of
31 the vertical stress function is in good agreement with the available experimental data.

32 It was found that the form of the transverse loading diagram has a significant effect on the degree of the
33 stress state of the soil. At the same average contact pressures, the parabolic shape of the loading
34 diagram, which is characteristic of tires with reduced internal air pressure, has the smallest effect on the
35 soil.

36 The method can serve as the basis for predicting the degree of soil compaction and the intensity of
37 rutting, as well as the environmental consequences of the operation of forest machines.

38 **Keywords**

39 Soil mechanics; Water-saturated soil; Environmental impact of vehicle; Forest vehicle; The first
40 boundary value problem; The finite element method. Level lines of a function.

Introduction

The result of the harmful environmental impact of the skidder on the ground is soil compaction, destruction of sod cover, and rut formation. As shown by numerous observations in the USA, Canada and other countries, the use of a wheeled skidder in logging leads to soil compaction and, as a consequence, to a decrease in forest productivity. The operation of the machine causes compaction and destruction of the sod cover, which serves as the most important source of plant nutrition. There is a change in biogeochemical cycles, and seed germination worsens within the framework of natural reforestation.

Destruction of the upper sod layer, saturated with organic matter, occurs as a result of deepening the lugs and wheel slip. As the analysis of the impact of the wheel on the ground shows, the most important factors affecting the environmental consequences of movement are, on the one hand, the physical and mechanical properties of the soil, on the other hand, the ability of the wheel to realize the required traction force with minimal slipping and cause minimal soil compaction.

When solving the problem of reducing the impact of the wheel on the soil and assessing its state after the passage of the machine, the question naturally arises of identifying the factors affecting the deformation and compaction of the soil, and finding the mathematical relationships between them. The existing mathematical models of the interaction of the wheel with the ground are usually based on a one-dimensional stress distribution function over depth, which is obtained by processing the results of stamping tests [8]. With this approach, it is impossible to assess the plane and spatial phenomena, including the distribution of compaction zones under the wheel and edge effects that cause lateral uplift of the soil. In addition, the whole principle of constructing the model is based on the mechanical transfer of the results of stamp tests to the wheel rolling process, it does not reflect the dynamics of the phenomenon, and the complication of the model by the introduction of correction factors for the geometric parameters of the contact patch and the time of application of the load does not contribute to

65 an increase in the accuracy of the solution, since their influence on the final result is nullified by
66 averaging the load over the contact patch and the accuracy of obtaining soil characteristics. Therefore,
67 it is necessary to look for new methods of constructing a mathematical model.

68 The basis for the construction of a mathematical model was a well-developed theory of soil mechanics.
69 Its methods have been successfully applied in practice for a long time. There are proven methods for
70 obtaining the required characteristics of soils and an extensive data on them.

71 The mathematical model, together with its software implementation, allows:

72 1) To judge the influence of the design features of the wheels and the nature of the vertical load on the
73 distribution of stresses in the soil.

74 2) Take into account the anisotropy of soil properties.

75 3) Simulate movement on ice and swamp.

76 4) Assess the ability and environmental impact of vehicle on soft ground.

77 5) Predict the degree of soil compaction and the intensity of rutting during the operation of the forest
78 machine.

79 ***1. Basic concepts of the physical and mechanical properties of soil***

80 By their nature, soils are divided into two main classes: sands are products of mechanical destruction of
81 basic rocks, and clays are products of chemical destruction of basic rocks. Sands and clays differ
82 greatly in their physical and mechanical properties.

83 In nature, soils of mixed origin are usually found. They exhibit intermediate properties of sand and clay
84 and are called, respectively, sandy loam, loam, etc.

85 All qualitative differences in soil properties are determined by the size and shape of the particles
86 forming them. Of great importance in the manifestation of these properties is the water in the gaps

87 between the particles. The gas in the soil (air, methane, water vapor) also strongly affects the properties
88 of the soil.

89 Sands consist of particles having the shape of grains with a diameter of 0.5 - 2 mm (coarse sand) to 0.1
90 - 0.05 mm (fine sand) [3]. Clay particles are in the form of plates with a thickness of not more than 1
91 micron.

92

93 Let us introduce the notation.

94

95 V - some volume of soil;

96

97 V_p - pore volume;

98

99 V_s - volume of solid particles;

100

101 $V = V_p + V_s$;

102

103 $n = \frac{V_p}{V}$ - soil porosity;

104

105 $m = \frac{V_s}{V}$ - the volume of solid particles per unit volume of soil;

106

107 $n + m = 1$;

108

109 $\varepsilon = \frac{V_p}{V_s} = \frac{n}{m}$ - coefficient of porosity.

110

111

Compressibility of soils

112

113 Due to the low permeability of solid soil particles, compression deformation occurs mainly due to a
114 change in porosity. The relationship between the coefficient of porosity ε and compressive stresses
115 σ is obtained using uniaxial compression devices. The curve is shown in Figure 1.1.

116

117

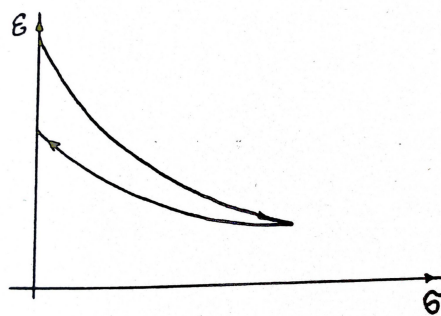


Figure 1.1: Compression curve

119

120 On small intervals of stresses change, it is approximated by a straight line

121

$$\varepsilon = -a\sigma + A \quad (1)$$

122 With a large number of loading and unloading, the soil becomes practically elastic.

123

124

Weakly compacted clays	0.10 - 0.01
Compacted clays	0.005 - 0.001

Compaction factors $a, \text{cm}^2/\text{kg}$ (according to Florin)

125

126

127

Sands	0.54 - 0.82
Compacted clays	0.67 - 1.2
Silt	1.00 - 3.00
Loams and clays	0.67 - 1.00

Porosity coefficients ε (according to Florin)

128

129

Filtration properties of soils

130

131 The filtration rate is defined in soil mechanics as the flow rate of water through a unit of the
 132 geometrical area of the soil section. Darcy's law establishes a relationship between the filtration rate
 133 u and the fluid pressure gradient H :

$$134 \quad u = -k \frac{\partial H}{\partial s} ,$$

135 where k is the filtration coefficient [cm / s].

136 H is determined in hydraulics by the formula:

137

$$138 \quad H = \frac{P}{\gamma} + z , [\text{cm}]$$

139

140 where P is the pressure in the liquid [kg/cm^2],

141

142 γ - specific gravity of the liquid [kg/cm^3],

143

144 z - the height of this point above the zero mark [cm].

145

146 The actual speed of water relative to immobile soil grains is determined by the formula:

147

148
$$u_a = \frac{u}{n},$$

149

150 where is n the porosity of the soil (see above).

151 In the case of movement of soil grains towards the liquid at a speed, v_a Darcy's law is written in the

152 form:

153

$$u_a - v_a = -\frac{k}{n} \frac{\partial H}{\partial s} \Rightarrow u - \varepsilon v = -k \frac{\partial H}{\partial s}. \quad (2)$$

154

Sands	$10^{-2} - 10^{-3}$
Clays	$10^{-6} - 10^{-8}$

Filtration coefficient k , cm/s (according to Florin)

155

156

157 **Understanding stresses in soil**

158

159 Consider the case of deformation propagation in one plane. Let's select an elementary parallelepiped
 160 and call the ratio of the force acting on an elementary area to its area stress. Then, on the sections of the
 161 parallelepiped, inclined at different angles, we will get different values of stresses. The stress vector
 162 coincides in direction with the force vector and it can be decomposed into normal and tangential
 163 components: σ_n and τ (Figure 1.2).

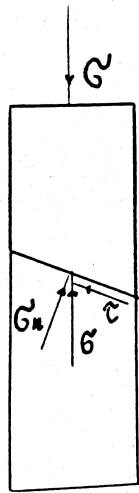


Figure 1.2 Plane stresses

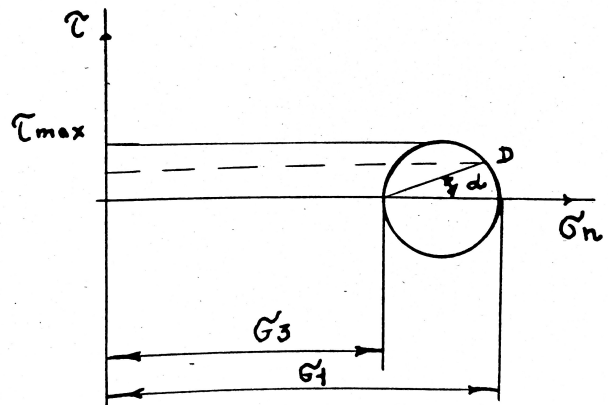


Figure 1.3 Mohr's circle

164

165 Let us introduce a rectangular coordinate system XoZ and denote the stresses acting along the oX and
 166 oZ axes, respectively, σ_x and σ_z .

167 Let only normal stress act in some section, and there is no tangential stress. This normal stress is called
 168 the principal one. The largest and the smallest normal stresses acting in a given section are the principal

169 ones. They are denoted by σ_1 and σ_3 respectively.

170 It is convenient to determine the stress distribution in the sections of an elementary parallelepiped using
171 Mohr's circles (Figure 1.3).

172 It can be seen from the figure that in the section drawn at an angle α , the values of the normal and
173 tangential stresses are determined by the coordinates of the point D on the circle. The maximum shear
174 stress in absolute value is achieved at $\alpha = \pm \pi/4$.

175

176 **The concept of soil strength**

177

178 In soil mechanics, the main indicators of strength are considered to be the shear resistance of the soil.

179 The maximum shear stress is determined from the equation:

180

$$\tau = c + \sigma_n \tan \varphi, \quad (3)$$

181 where c is called adhesion, and φ is the angle of internal friction. For sands $c=0$, therefore

182 $\tau = \sigma_n \tan \varphi$. The φ angle for sands is a constant value, while for clays the cohesion and the

183 angle of internal friction depend on the density and moisture. After preliminary compaction of the soil,

184 an increase in adhesion and a decrease in the angle of internal friction are observed, this is due to an

185 irreversible decrease in the coefficient of porosity ε , as a result of which the molecular forces of

186 interaction between particles increase [6].

187 From equation (3), you can determine the straight lines, which are called the lines of destruction. For a

188 given value σ_1 , construct a Mohr circle so that it touches these lines (Figure 1.4).

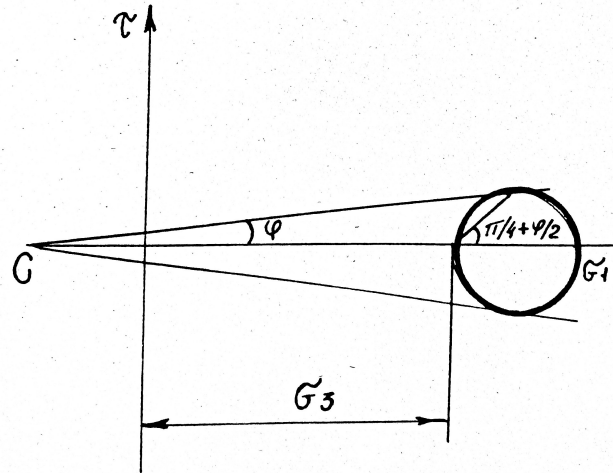


Figure 1.4 Plastic limit equilibrium

189

190

191 The slope of the fracture planes can now be determined. It makes an angle $\pi/4 + \varphi/2$ to the line of
 192 action of the lowest principal stress. At this moment, the principal stresses satisfy the equation

193

$$\sigma_1 = 2c\sqrt{\lambda_\varphi} + \sigma_3\lambda_\varphi, \quad (4)$$

194

195 where $\lambda_\varphi = \tan^2(\pi/4 + \varphi/2)$, and the soil massif is in a state of so-called plastic limiting equilibrium
 196 [9]. The effect of the hydrostatic pressure of water in the pores of the soil should also be taken into
 197 account, therefore, the so-called effective stress, which is perceived by the skeleton of the soil, should
 198 be substituted in formulas (3) and (4), and their values are less than the actual stresses by the value of
 199 the pore pressure of water. The sine of the largest deviation of the total stress vector can be represented
 200 as:

201

$$\sin \theta_{max} = \frac{\sqrt{(\sigma_x - \sigma_z)^2 + 4\tau_{xz}^2}}{\sigma_z + \sigma_x + 2c/\tan \varphi}.$$

Deformation modulus and Poisson's ratio

When compressing a soil sample in a compression device, transverse deformations of the soil are impossible. In this case, the lateral pressure coefficient ζ is determined by the formula: $\zeta = \frac{\sigma_x}{\sigma_z}$. In soil mechanics, it is assumed that porosity depends only on the sum of the principal stresses, and not on their ratios. This assumption is based on the approximation of the real stress-strain curve by a straight line with sufficient accuracy for practical calculations. Because of this, we write formula (1) for the case of a biaxial stress state (plane problem):

$$\varepsilon = -a \frac{\theta}{1 + \zeta} + A, \quad (5)$$

here $\theta = \sigma_x + \sigma_z$ is the sum of the principal stresses.

The deformation modulus $E(\varepsilon)$ is determined in soil mechanics from the expression:

$$de_x = \frac{d\sigma_x - \nu d\sigma_z}{E(\varepsilon)},$$

where σ_x and σ_z is the increment in stresses, that caused de_x - the strain increment along the Ox axis.

Poisson's ratio ν is defined through the lateral pressure coefficient ζ : $\nu = \frac{\zeta}{1 + \zeta}$.

If we take the dependence $\varepsilon = \varepsilon(\theta)$ as linear, for example, in the form (5), we obtain

$$E = \frac{\beta(1 + \varepsilon)}{a},$$

223 where $\beta = \frac{(1-\xi)(1+2\xi)}{(1+\xi)}$.

224

Sands	0.40-0.42
Clays	0.70-0.75

Lateral pressure coefficient (according to Florin)

225

226 The above expressions for the deformation moduli make it possible, in the case of a nonlinear
227 relationship between stresses and strains, to determine the modulus value for any given stress state.

228 However, in many cases it is more convenient to use the so-called average deformation modulus

229

230 $E_{avg} = \frac{\beta(1+\epsilon_1)}{a}$, where ϵ_1 is the initial porosity coefficient.

231

232 It was shown (N.M. Gersevanov) the constancy of E_{avg} for plastic soils in a small range of load
233 variation, which indicates a linear relationship between stresses in the skeleton and its deformations,
234 and this shows that the formulas of the theory of elasticity are applicable to the calculations of stresses
235 and deformations in the soil skeleton.

236 In conclusion, let us consider the case of applying a vertical load along the rectilinear boundary of a
237 linearly deformed medium. In this case [10]:

238

$$\sigma_x = \frac{1}{2}\theta + \frac{1}{2}z \frac{\partial \theta}{\partial z}$$

$$\sigma_z = \frac{1}{2}\theta - \frac{1}{2}z \frac{\partial \theta}{\partial z} \quad (6)$$

$$\tau_{xz} = -\frac{1}{2}z \frac{\partial \theta}{\partial x}$$

239 The stress components are determined by the formulas:

240

$$241 \quad \sigma_x = \lambda e + \nu \varepsilon_x$$

$$242 \quad \sigma_z = \lambda e + \nu \varepsilon_z \quad ,$$

$$243 \quad \text{where } \varepsilon_x = \frac{\partial u_1}{\partial x} \quad , \quad \varepsilon_z = \frac{\partial u_3}{\partial z} \quad , \quad \lambda = \frac{\nu E}{(1+\nu)(1-2\nu)} \quad , \quad e = \varepsilon_x + \varepsilon_z \quad ,$$

244 u_1 и u_3 - displacement components.

245

$$246 \quad \tau_{xz} = \nu \gamma_{xz} \quad ,$$

$$247 \quad \text{where } \gamma_{xz} = \frac{\partial u_1}{\partial z} + \frac{\partial u_3}{\partial x} \quad .$$

248

249 For a general model of a linearly deformable medium, the stresses in the soil skeleton must satisfy the

250 equations [10]:

251

$$\frac{\partial \sigma_x}{\partial x} + \frac{\partial \tau_{xz}}{\partial z} + X = 0 \quad (7)$$

252

$$\frac{\partial \tau_{xz}}{\partial x} + \frac{\partial \sigma_z}{\partial z} + Z = 0 \quad , \quad (8)$$

253

254 where X и Z - components of volumetric forces,

255 along with the equation

256

$$\Delta(\sigma_x + \sigma_z) = -\frac{1}{1-\nu} \left(\frac{\partial X}{\partial x} + \frac{\partial Z}{\partial z} \right) \quad , \quad (9)$$

257

258 where ν - коэффициент Пуассона ;

259 Δ - оператор Лапласа.

260 ***2. Mathematical formulation of the compaction problem***

261 **2.1. The Simplest One-Dimensional Compaction Problem**

262 Key assumptions:

263 a) We consider models of a two-component soil consisting of solid particles and water filling its pores.

264 This model is called soil mass. “The question may arise: in what cases, in practice, are we dealing with

265 a soil mass? ... As for the ground lying above the groundwater level, in the vast majority of cases it is a

266 soil mass, that is, one in which all voids are filled with water due to the capillary rise of water in the

267 fine pores of the soil. In clays, the length of the capillary rise of water can reach a height of over 300 m

268 above the groundwater level.

269 In order to judge whether we have a soil mass above the groundwater level, we can be guided by the

270 following signs: in all cases when the soil is in a fluid, plastic and semi-solid state, we are dealing with

271 a soil mass. Only when the soil passes from a semi-solid state to a solid state does air penetrate into the
 272 pores of the soil and partially fill the voids of the soil skeleton. The transition from solid to solid is
 273 characterized by a sharp change in the color of the soil. ... To determine the condition of the soil, i.e.
 274 whether it is fluid, plastic or semi-solid, there are fully developed laboratory methods ... "(N.M.
 275 Gersevanov, [2, p. 145]).

276 b) The change in porosity occurs only due to the dense packing of soil particles;

277 c) The filtration coefficient does not depend on the stress state.

278 Basic equations

279 1. Equations of continuity for solid and liquid soil components.

280

$$\frac{\partial u_z}{\partial z} + \frac{\partial n}{\partial t} = 0, \quad (1)$$

281

$$\frac{\partial v_z}{\partial z} + \frac{\partial m}{\partial t} = 0, \quad (2)$$

282 here, as before, v_z and u_z are the flow rates of the solid and liquid components along the oZ axis.

283 Adding equations (1), (2) and taking into account equality $n + m = 1$, we obtain

284

$$\frac{\partial u_z}{\partial z} + \frac{\partial v_z}{\partial z} = 0. \quad (3)$$

285

286 2. Darcy's dependency.

287

$$u_z - \varepsilon v_z = -k \frac{\partial H}{\partial z}. \quad (4)$$

288

289

290 3. Equilibrium equation.

291 Let σ - stress in the soil skeleton; p - pressure in water; σ^* and p^* - the corresponding
292 values in a state of complete stabilization.

$$\sigma + p = \sigma^* + p^* . \quad (5)$$

293 That is the sum of stress and pressure is a constant.

294 Differentiate (4) by z :

$$\frac{\partial u_z}{\partial z} - \frac{\partial \epsilon}{\partial z} v_z - \epsilon \frac{\partial v_z}{\partial z} = - \frac{\partial}{\partial z} \left(k \frac{\partial H}{\partial z} \right) ,$$

296

297 considering (3):

$$v_z \frac{\partial \epsilon}{\partial z} + (1 + \epsilon) \frac{\partial v_z}{\partial z} = \frac{\partial}{\partial z} \left(k \frac{\partial H}{\partial z} \right) .$$

299 Further, taking into account (2) and the relationship between ϵ and m from Section 1, we obtain:

$$\frac{\partial v_z}{\partial z} = - \frac{\partial m}{\partial t} = - \frac{\partial}{\partial t} \left(\frac{1}{1 + \epsilon} \right) = \frac{1}{(1 + \epsilon)^2} \frac{\partial \epsilon}{\partial t} ;$$

301

$$v_z \frac{\partial \epsilon}{\partial z} + (1 + \epsilon) \frac{\partial v_z}{\partial z} = \frac{\partial}{\partial z} \left(k \frac{\partial H}{\partial z} \right) .$$

303 Further, as shown in [4],

$$v_z \frac{\partial \epsilon}{\partial z} = o \left(\frac{\partial \epsilon}{\partial t} \right)$$

305 and the error from replacement $[1 + \epsilon(t, z)]$ by $[1 + \epsilon(t, z)]$ (ϵ is the average porosity in the

306 considered compaction range) is less than the error of the laboratory determination of the filtration
 307 coefficient k .

308 In view of the above

$$309 \quad \frac{\partial \varepsilon}{\partial z} = (1 + \varepsilon) \frac{\partial}{\partial z} \left(k \frac{\partial H}{\partial z} \right)$$

310

$$311 \quad \frac{\partial \varepsilon}{\partial t} = \frac{d \varepsilon}{d \sigma} \frac{\partial \sigma}{\partial t} = -a \left(-\frac{\partial p}{\partial t} \right) = a \gamma \frac{\partial H}{\partial t} .$$

312

313 Here we used equation (1) from Section 1 and equilibrium equation (5). We will finally write down

314

315

316

$$\frac{\partial H}{\partial t} = \frac{(1 + \varepsilon)}{a \gamma} \frac{\partial}{\partial z} \left(k \frac{\partial H}{\partial z} \right) . \quad (6)$$

317 The resulting equation is equivalent in form to the equation of heat conduction and diffusion.

318 Next, the initial and boundary conditions are assigned:

$$319 \quad t=0, \quad H=H(Z) ;$$

320

$$321 \quad t>0, \quad z=0: \quad H=\lambda(t), \quad z=z^*: \quad H=\mu(t) .$$

322

323 Example. Let the distributed load $q: \quad H_o=q/\gamma$ be instantaneously applied at the initial moment

324 $t=0$. If the layers $z=0$ and $z=z^*$ are also permeable, then when $t>0$:

$$325 \quad z=0, \quad H=0; \quad z=z^*, \quad H=0 ,$$

326 For waterproof layers $\frac{\partial H}{\partial z}=0$.

327 The solution of equation (6) together with the given initial and boundary conditions is found by known
328 methods, for example, by the method of separation of variables (by the Fourier method). The stress
329 distribution $\sigma(z, t)$ is determined from equation (5):

330
$$\sigma + p = \text{const} = q$$

331

332
$$\sigma = q - p = q - \gamma H$$
 .

333

334 The amount of compaction can be found by the formula:

335
$$s(t, h) = \int_0^h e_z(t, z) dz$$
 ,

336 where e_z is the compaction of the layer with the coordinate z , according to the results of Section
337 1

338
$$e_z = \frac{a}{1 + \varepsilon} \sigma$$
 ;

339 h - active compaction depth, can be determined in the following way:

340 make up a sequence $(h_k), k=0,1,2, \dots$ and determine h_l from the condition:

341
$$\frac{|s(t, h_{l-1}) - s(t, h_l)|}{s(t, h_l)} \leq \delta$$

342 Where δ is the specified accuracy. Thus, the problem of compaction in the one-dimensional case can
343 be considered solved.

2.2. Plane and spatial problems of compaction

The assumptions are the same as in the previous paragraph. First, consider the planar compaction problem (XoZ plane).

Basic equations.

1. Equations of continuity

$$\frac{\partial u_x}{\partial x} + \frac{\partial u_z}{\partial z} + \frac{\partial n}{\partial t} = 0 \quad (1)$$

$$\frac{\partial v_x}{\partial x} + \frac{\partial v_z}{\partial z} + \frac{\partial m}{\partial t} = 0 \quad (2)$$

Add equations (1), (2)

$$\frac{\partial (u_x + v_x)}{\partial x} + \frac{\partial (u_z + v_z)}{\partial z} = 0 \quad (3)$$

2. Darcy's dependence

$$u_x - \varepsilon v_x = -k \frac{\partial H}{\partial x} \quad (4)$$

$$u_z - \varepsilon v_z = -k \frac{\partial H}{\partial z} \quad (5)$$

3. Equilibrium equations

360

$$\sigma_x + p = \sigma_x^* + p^* \quad (6)$$

361

$$\sigma_z + p = \sigma_z^* + p^* \quad (7)$$

362

$$\tau_{xz} = \tau_{xz}^* \quad (8)$$

363

364 Here τ_{xz} are the shear stresses. It is assumed that the tangential load is instantly perceived by the
365 skeleton and is not transmitted to the water.

366 Differentiate (4) by x , (5) by z and add up:

367

$$\frac{\partial u_x}{\partial x} + \frac{\partial u_z}{\partial z} - \varepsilon \left(\frac{\partial v_x}{\partial x} + \frac{\partial v_z}{\partial z} \right) = - \left[\frac{\partial}{\partial x} \left(k \frac{\partial H}{\partial x} \right) + \frac{\partial}{\partial z} \left(k \frac{\partial H}{\partial z} \right) \right] \quad .$$

369

370 Comment. Discarded terms $\frac{\partial \varepsilon}{\partial z} v_z$ and $\frac{\partial \varepsilon}{\partial x} v_x$.

371

372 Taking into account (3), we obtain

373

$$(1 + \varepsilon) \left(\frac{\partial v_x}{\partial x} + \frac{\partial v_z}{\partial z} \right) = \frac{\partial}{\partial x} \left(k \frac{\partial H}{\partial x} \right) + \frac{\partial}{\partial z} \left(k \frac{\partial H}{\partial z} \right) \quad ,$$

375

376 where the value $1 + \varepsilon$ is a constant (see section 2.1).

377 Further, from (2) we have

378

$$\frac{\partial v_x}{\partial x} + \frac{\partial v_z}{\partial z} = - \frac{\partial m}{\partial t} = \frac{1}{(1 + \varepsilon)^2} \frac{\partial \varepsilon}{\partial t} \quad ,$$

379 taking this into account, we get

380

$$\frac{\partial \varepsilon}{\partial t} = (1 + \varepsilon) \left[\frac{\partial}{\partial x} \left(k \frac{\partial H}{\partial x} \right) + \frac{\partial}{\partial z} \left(k \frac{\partial H}{\partial z} \right) \right] . \quad (9)$$

381

382 Next, we use equation (5) from Section 1.1. We have

383

$$\frac{\partial \varepsilon}{\partial t} = \frac{d \varepsilon}{d \sigma} \frac{\partial \sigma}{\partial t} = - \frac{a}{1 + \xi} \frac{\partial \theta}{\partial t} .$$

385

386 From equations (6) and (7) we obtain

387

$$\theta = \sigma_x + \sigma_z = \theta^* = \sigma_x^* + \sigma_z^* - 2(p - p^*)$$

389 so

$$\frac{\partial \theta}{\partial t} = -2 \frac{\partial p}{\partial t} = -2 \gamma \frac{\partial H}{\partial t} .$$

391

392 Let us finally write equation (9) in the form:

393

$$\frac{\partial H}{\partial t} = \frac{(1 + \varepsilon)(1 + \xi)}{2 \gamma a} \left[\frac{\partial}{\partial x} \left(k \frac{\partial H}{\partial x} \right) + \frac{\partial}{\partial z} \left(k \frac{\partial H}{\partial z} \right) \right] . \quad (10)$$

394

395 Reasoning quite similarly in the case of a triaxial stress state, we arrive at the equation:

396

$$\frac{\partial H}{\partial t} = \frac{(1 + \varepsilon)(1 + 2\xi)}{3 \gamma a} \left[\frac{\partial}{\partial x} \left(k \frac{\partial H}{\partial x} \right) + \frac{\partial}{\partial y} \left(k \frac{\partial H}{\partial y} \right) + \frac{\partial}{\partial z} \left(k \frac{\partial H}{\partial z} \right) \right] . \quad (11)$$

397

398 Let us assume that the filtration coefficient k does not change during the compaction process. Then
 399 we have:

$$\frac{\partial H}{\partial t} = K \Delta H \quad . \quad (12)$$

400

401 Where Δ is the Laplace operator,

402

$$403 \quad K = \frac{(1+\varepsilon)(1+\xi)}{2 \gamma a} k \quad - \text{ for a plane problem}$$

404

$$405 \quad K = \frac{(1+\varepsilon)(1+2\xi)}{3 \gamma a} k \quad - \text{ for a spatial problem.}$$

406

Initial conditions

407 Note that the initial heads distribution function H_o satisfies the Laplace equation

408

$$\Delta H_o = 0 \quad . \quad (13)$$

409

410 This equation is a consequence of the fact that at the initial moment of load application

411

$$412 \quad \frac{\partial v_x}{\partial x} = \frac{\partial v_y}{\partial y} = \frac{\partial v_z}{\partial z} = 0 \quad .$$

413

414 We find the initial pressure distribution from (6) and (7):

415 in the case of the plane problem

$$P_o = \frac{1}{2} \theta_o^* + P_o^* , \quad (14)$$

416 for a spatial task

417

$$P_o = \frac{1}{3} \theta_o^* + P_o^* . \quad (15)$$

418 Here, as before, θ_o^* denotes the sum of normal stresses in a stabilized state, P_o^* is the final pressure

419 distribution. We accept further $P_o^* = 0$.

420 Thus, to determine the initial distribution of the pressure, it is necessary to solve problems (7), (8) and

421 (9) of the theory of elasticity (Section 1).

422 The initial stress distribution is determined from (6), (7), (14), (15)

423 For a planar problem

$$424 \quad \sigma_{xo} = \frac{1}{2} (\sigma_x^* - \sigma_z^*)$$

$$425 \quad \sigma_{zo} = \frac{1}{2} (\sigma_z^* - \sigma_x^*)$$

$$426 \quad \tau_{xzo} = \tau_{xz}^* .$$

427 For a spatial problem

$$428 \quad \sigma_{xo} = \sigma_x^* - \frac{1}{3} \theta_o^*$$

$$429 \quad \sigma_{yo} = \sigma_y^* - \frac{1}{3} \theta_o^*$$

$$430 \quad \sigma_{zo} = \sigma_z^* - \frac{1}{3} \theta_o^*$$

$$431 \quad \tau_{xzo} = \tau_{xz}^* , \quad \tau_{xyo} = \tau_{xy}^* , \quad \tau_{yzo} = \tau_{yz}^* .$$

432

433

Border conditions

434 On the permeable sections of the boundary surface, the values of the pressure function are equal to

435 zero: $H=0, x \in \Gamma$. In watertight areas, the pressure gradient value is zero:

436
$$\frac{\partial H}{\partial n}=0, x \in \Gamma$$
 .

437 In addition, in the case of compaction of heterogeneous soil, the conjugation conditions must be met at

438 the border of adjacent media:

439
$$H_1(x, t)|_S = H_2(x, t)|_S ;$$

440
$$k_1\left(\frac{\partial H_1}{\partial n}\right) = k_2\left(\frac{\partial H_2}{\partial n}\right) .$$

441

442 Example. The plane problem of compaction of isotropic soil with an arbitrary vertical load. We find the

443 initial stress distribution from equation (6) in Section 1 and from equations (6), (7), (8):

444

$$\begin{aligned}
\sigma_{xo} &= \frac{1}{2}(\sigma_x^* - \sigma_z^*) = \frac{1}{2}z \frac{\partial \theta^*}{\partial z} = z \frac{\partial P_o}{\partial z} \\
\sigma_{zo} &= \frac{1}{2}(\sigma_z^* - \sigma_x^*) = -z \frac{\partial P_o}{\partial z} \\
\tau_{xzo} &= \tau_{xz}^* = \frac{1}{2}z \frac{\partial \theta^*}{\partial x} = -z \frac{\partial P_o}{\partial x}
\end{aligned}
\tag{16}$$

445

446 To determine P_o , it is necessary to solve the following problem:

447

$$\Delta P_o = 0 ,$$

448 $z=0, x \in D$ $P_o = q(x)$ - given load,

$$\begin{aligned} x \notin D \quad P_o = 0; \\ x \rightarrow \pm \infty, \quad z \rightarrow \pm \infty, \quad P_o = 0 \end{aligned} \quad (17)$$

449

450 Consider a more general first boundary value problem:

$$\begin{aligned} Lu = -f(M), \quad (M \in D) \\ u|_S = \varphi(M) \end{aligned} \quad (18)$$

451 In the original problem

$$452 \quad u \equiv H, \quad Lu = \Delta u = \frac{\partial^2 u}{\partial x^2} + \frac{\partial^2 u}{\partial z^2};$$

$$453 \quad f(M) = f(x, z) = 0, \quad (M \in D);$$

$$454 \quad \varphi(M) = \varphi(x, z) \equiv \begin{cases} 0, & z = 0, x \notin [-a, a] \\ q(x), & z = 0, x \in [-a, a] \\ 0, & z \rightarrow +\infty, x \rightarrow \pm\infty \end{cases},$$

455 where $q(x) = \gamma q(x)$ is the diagram of the load distribution, $2a$ is the contact width (Figure 2.1).

456

457

458

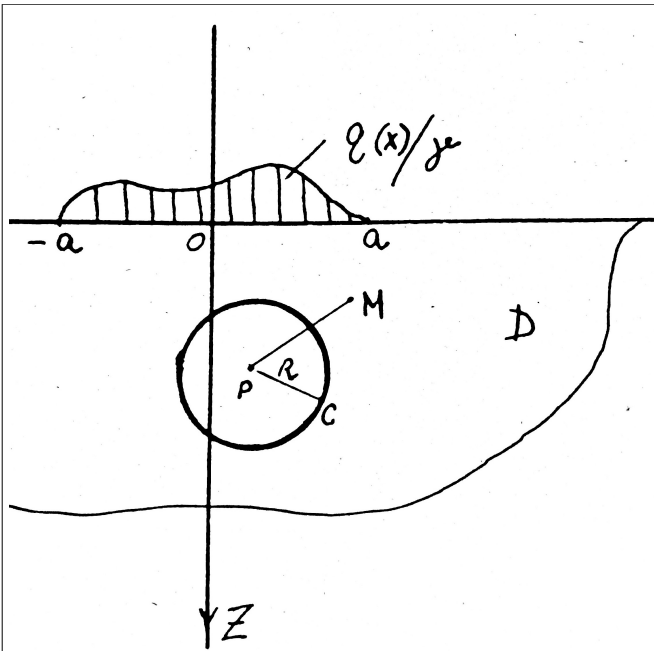


Figure 2.1 On the definition of the Green's function

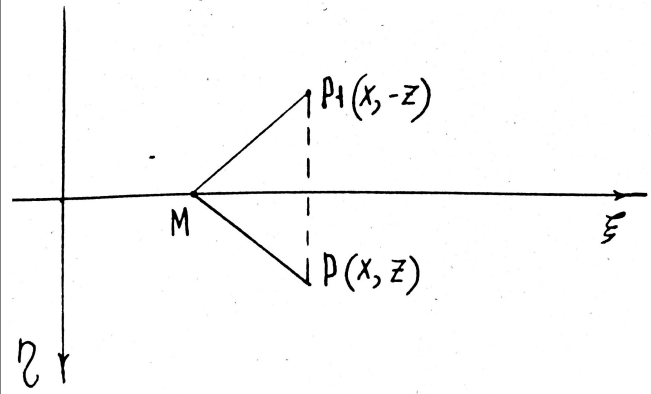


Figure 2.2 Reflection method

459

460 To solve problem (18), the method of Green's functions is used, the solution has the form [5]:

461

$$u(P) = - \int_S \varphi \frac{\partial G}{\partial n} dS_M$$

462 where $G = G(M, P)$ is the solution to an equation of a special form:

463

$$\begin{cases} \Delta G = -\delta(M, P) & (M \in D) \\ G|_S = 0 \end{cases} \quad (19)$$

464

465 Here $\delta(M, P)$ is the Dirac δ - function. Solution (19) is presented in the form:

466

467

$$G(M, P) = \psi(\Gamma_{MP}) + V(M, P) ,$$

468

469 where V is harmonious at D (i.e. $\Delta V=0, M \in D$), and $\psi(\Gamma_{MP})$ has a singularity at the point
 470 P and at $\Gamma_{MP}=0$

471

$$\Delta \psi = -\delta(M, P) \quad . \quad (20)$$

472

473 We integrate (20)

$$474 \quad \int_{S_P^R} \Delta \psi ds = -1 \quad (\delta \text{ - function property}).$$

475 Using Green's formula, we pass to the integral over a circle centered at the point P of radius R

476 (see Figure 2.1):

$$\begin{aligned} 477 \quad \oint_C \frac{\partial \psi}{\partial n} ds &= \oint_C \frac{d\psi}{dr} ds = \frac{d\psi}{dr} \Big|_R \cdot 2\pi R = -1 \\ d\psi(R) &= -\frac{1}{2\pi} \frac{dR}{R} \Rightarrow \psi(R) = -\frac{1}{2\pi} \ln \frac{1}{R} \quad . \\ \Rightarrow G(M, P) &= \frac{1}{2\pi} \ln \left(\frac{1}{\Gamma_{MP}} \right) + V(M, P) \end{aligned}$$

478

479 For our case $V(M, P)$ is determined by the method of reflections (Figure 2.2).

480 Due to the fact that on the boundary of the half-plane $G(M, P)=0$, it follows that

$$481 \quad V(M, P) = -\frac{1}{2\pi} \ln \left(\frac{1}{\Gamma_{MP_1}} \right) \text{ is a harmonic function } \forall M \in D \quad .$$

$$482 \quad \Rightarrow G(M, P) = \frac{1}{2\pi} \ln \left(\frac{1}{\Gamma_{MP}} \right) - \frac{1}{2\pi} \ln \left(\frac{1}{\Gamma_{MP_1}} \right) \quad ,$$

483 or in coordinates $x, z, \xi, \eta: (M(\xi, \eta), P(x, z))$:

$$484 \quad G(M, P) = \frac{1}{2\pi} \ln \left(\frac{1}{\sqrt{(x-\xi)^2 + (z-\eta)^2}} \right) - \frac{1}{2\pi} \ln \left(\frac{1}{\sqrt{(x-\xi)^2 + (z+\eta)^2}} \right)$$

485 $\Rightarrow u(P) = - \int_a^{-a} q(\xi) \frac{\partial G}{\partial \eta} \big|_{\eta=0} d\xi$, and it remains to find

486
$$\frac{\partial G}{\partial \eta} \big|_{\eta=0} = \frac{1}{2\pi} \ln \left(\frac{2z}{(x-\xi)^2 + z^2} \right) .$$

487 Thus, the solution (18) is:

488
$$H_o(x, z) = \frac{1}{\pi} \int_a^{-a} q(\xi) \frac{z}{(x-\xi)^2 + z^2} d\xi .$$

489 For the original problem, this is equivalent to the following expression:

490
$$H_o(x, z) = \frac{1}{\pi} \int_a^{-a} q(\xi) \frac{z}{(x-\xi)^2 + z^2} d\xi .$$

491 So found in the initial pressure distribution:

492
$$P_o(x, z) = \frac{Y}{\pi} \int_a^{-a} q(\xi) \frac{z}{(x-\xi)^2 + z^2} d\xi ,$$

493 where $q(\xi) = \frac{q(\xi)}{Y}$, that is, you can rewrite

494

$$P_o(x, z) = \frac{1}{\pi} \int_a^{-a} q(\xi) \frac{z}{(x-\xi)^2 + z^2} d\xi . \quad (21)$$

495

496 We find the initial stress distribution by the formulas (16):

497

$$\sigma_{xo} = z \frac{\partial P_o}{\partial z} = \frac{z}{\pi} \int_a^{-a} q(\xi) \frac{(x-\xi)^2 - z^2}{[(x-\xi)^2 + z^2]^2} d\xi$$

$$\sigma_{zo} = -\sigma_{xo} . \quad (22)$$

$$\tau_{xzo} = -z \frac{\partial P_o}{\partial z} = \frac{1}{\pi} \int_a^{-a} q(\xi) \frac{2z(x-\xi)}{[(x-\xi)^2 + z^2]^2} d\xi$$

498

499 The distribution of initial stresses and pressures for an arbitrary vertical load is shown in Figures 2.3
500 and 2.4.

501

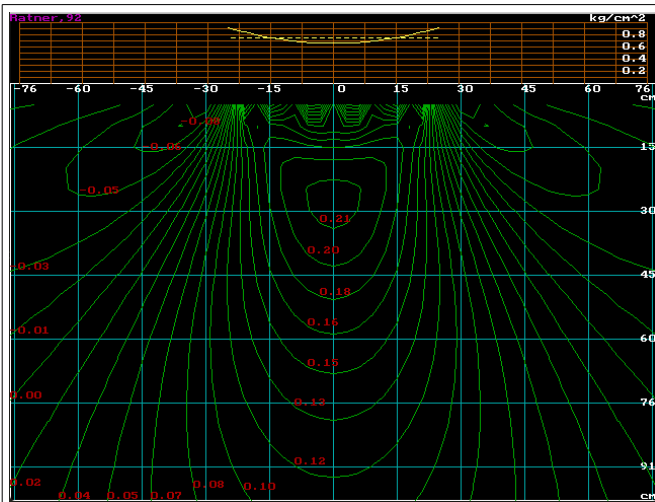


Figure 2.3 Distribution of initial stresses
(σ_{z0} , kg/cm^2) in a homogeneous environment

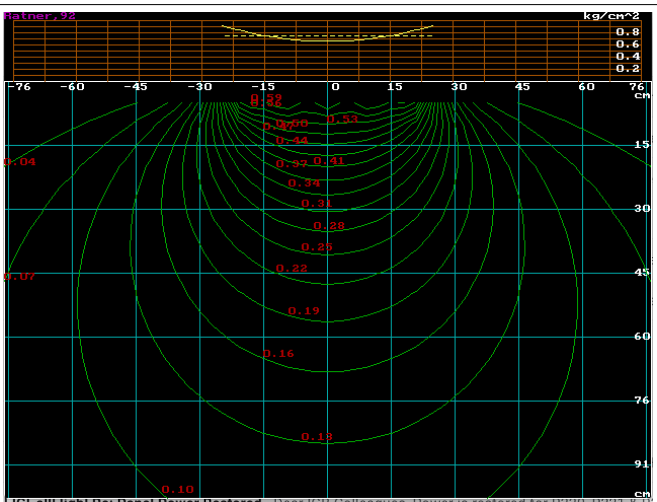


Figure 2.4 Distribution of initial pressures
(P_0 , kg/cm^2) in a homogeneous environment

502 **3. Finite-element solution of a multimodular problem of the theory of**
503 **elasticity**

504 The initial conditions of problem (12) in Section 2 are expressed in terms of the steady-state stress
505 distribution, the definition of which is devoted to this section.

506 Earlier it was indicated (Section 1) that the formulas of the theory of elasticity are formally applicable
507 to the calculation of stresses and strains in the soil skeleton, although in essence it means the presence
508 of not elastic, but a linear relationship between stresses and deformations.

509 Select a rectangular area on the half-plane and triangulate it (Figure 3.1).

510

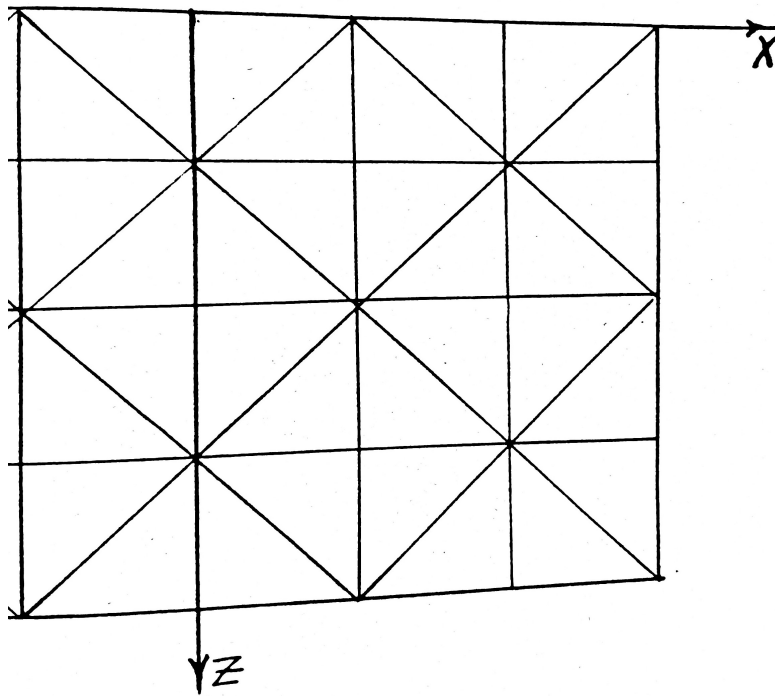


Figure 3.1 Area triangulation

513 Consider the four types of triangles used in the partition. The nodes are numbered clockwise (Figure
 514 3.2).

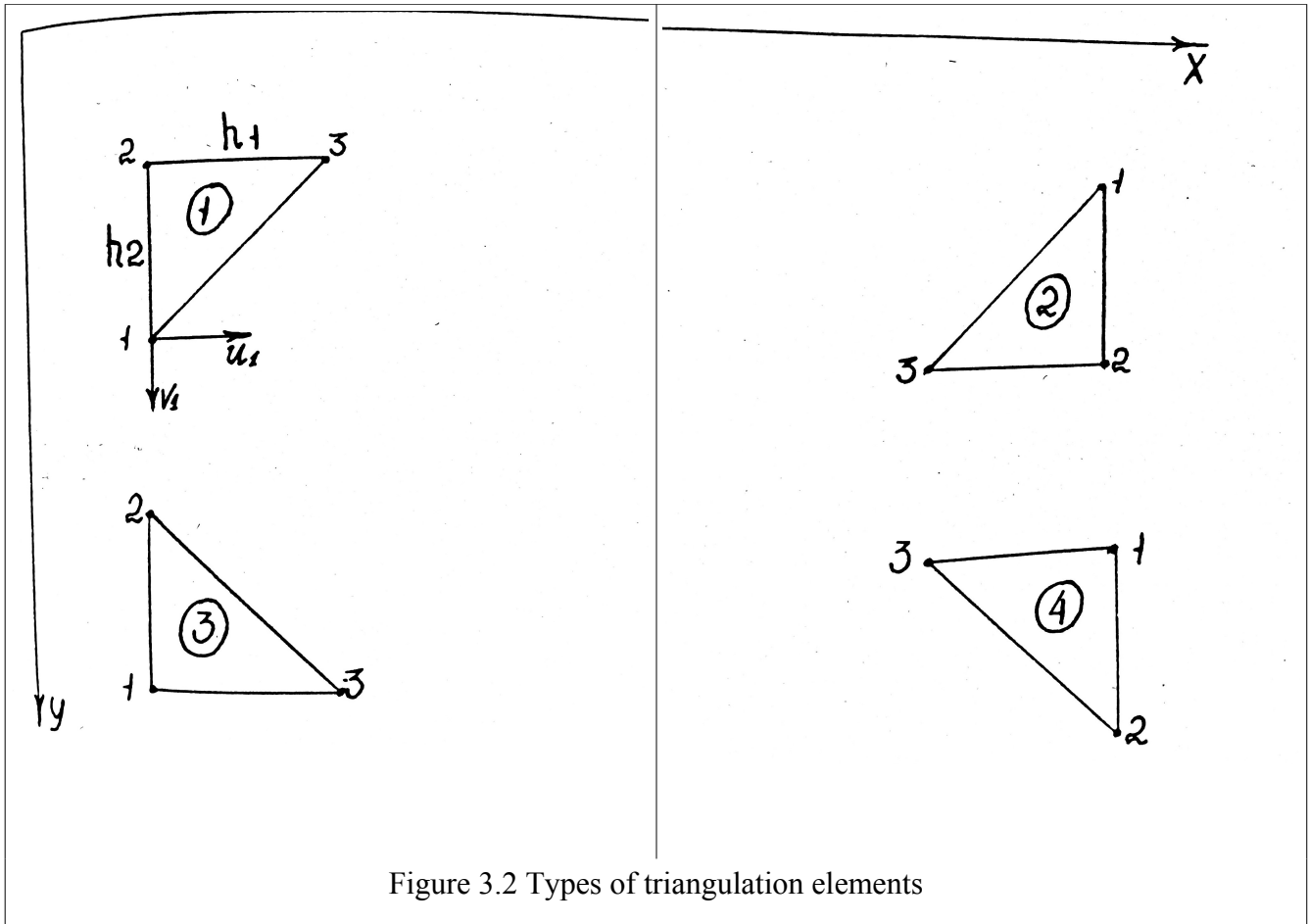


Figure 3.2 Types of triangulation elements

515 We denote the movement of the i -th node of a separate element through u_i and v_i . The
 516 displacements of the nodes belonging to the vertical boundaries of the half-plane are set to zero.
 517 The displacements of element points are expressed in terms of nodal displacements:

518

$$U_N = \Phi U \quad (1)$$

519

520 Where $U_N = \begin{bmatrix} U(x, y) \\ V(x, y) \end{bmatrix}$ - the vector of displacements;

521

$$\Phi = \begin{bmatrix} \varphi_1 & 0 & \varphi_2 & 0 & \varphi_3 & 0 \\ \varphi_1 & 0 & \varphi_2 & 0 & \varphi_3 & 0 \end{bmatrix} \quad \text{- shape matrix;}$$

522 $\varphi_1, \varphi_2, \varphi_3$ - form functions on an element;

523 $U = [u_1, v_1, u_2, v_2, u_3, v_3]^T$ - vector of nodal values of displacements on the element.

524 We carry out a functional expressing the potential energy of a deformed body:

$$I = \sum_{e=1}^{e=l} t_e \int_{\Omega_e} \frac{1}{2} \varepsilon^T \sigma d\Omega_e - \sum_{e=1}^{e=l} t_e \int_{\Gamma_e} U_N^T Q d\Gamma_e \quad . \quad 2$$

525 Here the contributions are summed over l - elements, each of them with thickness t_e , area Ω_e ;

526 $\varepsilon = (\varepsilon_x, \varepsilon_y, \gamma_{xy})^T$ - deformation vector,

527 $\sigma = (\sigma_x, \sigma_y, \tau_{xy})^T$ - stress vector,

528 $Q = (q_x, q_y)^T$ is the vector of the distributed load applied to the boundary Γ_e of the boundary

529 element e .

530 The relationship between stresses and deformation is expressed by Hooke's law [10]:

531

$$\sigma = D \varepsilon \quad . \quad 3$$

532

533 Here D is the elasticity matrix of the element:

$$534 \quad D = \frac{E}{1-\nu^2} \begin{bmatrix} 1 & \nu & 0 \\ \nu & 1 & 0 \\ 0 & 0 & (1-\nu)/2 \end{bmatrix} ,$$

535 where E is the modulus of deformation on the element,

536 ν - Poisson's ratio on the element.

537 The relationship between displacement and deformation is expressed by the formula [10]:

538

$$\varepsilon = \begin{bmatrix} \frac{\partial u}{\partial x} \\ \frac{\partial v}{\partial y} \\ \frac{\partial u}{\partial x} + \frac{\partial v}{\partial y} \end{bmatrix}$$

539 or, taking into account (1), we write

540

$$\varepsilon = B \cdot U \quad (4)$$

541

542 where

543

$$B = \begin{bmatrix} \frac{\partial}{\partial x} & 0 \\ 0 & \frac{\partial}{\partial y} \\ \frac{\partial}{\partial x} + \frac{\partial}{\partial y} \end{bmatrix} \cdot \Phi = \begin{bmatrix} \frac{\partial \varphi_1}{\partial x} & 0 & \frac{\partial \varphi_2}{\partial x} & 0 & \frac{\partial \varphi_3}{\partial x} & 0 \\ 0 & \frac{\partial \varphi_1}{\partial y} & 0 & \frac{\partial \varphi_2}{\partial y} & 0 & \frac{\partial \varphi_3}{\partial y} \\ \frac{\partial \varphi_1}{\partial y} & \frac{\partial \varphi_1}{\partial x} & \frac{\partial \varphi_2}{\partial y} & \frac{\partial \varphi_2}{\partial x} & \frac{\partial \varphi_3}{\partial y} & \frac{\partial \varphi_3}{\partial x} \end{bmatrix}.$$

544 We accept the functions of the shape of the element as linear and equal on the element to its barycentric

545 coordinates, and outside the element to zero:

546

$$\varphi_i = \frac{a_i x + b_i y + c_i}{2S}, i=1,2,3.$$

547

Where S is the area of the element,

548

$$\left. \begin{aligned} a_1 &= y_2 - y_3 \\ b_1 &= x_3 - x_2 \\ c_1 &= x_2 y_3 - x_3 y_2 \end{aligned} \right\} . \quad (5)$$

549

550 The coefficients $a_2, a_3, b_2, b_3, c_2, c_3$ are determined through the cyclic permutation of the indices in (5).

551 Then the matrix B will take the form:

552
$$B = \frac{1}{2S} \begin{bmatrix} a_1 & 0 & a_2 & 0 & a_3 & 0 \\ 0 & b_1 & 0 & b_2 & 0 & b_3 \\ b_1 & a_1 & b_2 & a_2 & b_3 & a_3 \end{bmatrix} .$$

553 Let's rewrite (2) taking into account (1), (3), (4):

554

$$I = \sum_{e=1}^{e=l} t_e \int_{\Omega_e} \frac{1}{2} U^T B^T D \cdot B \cdot U d\Omega_e - \sum_{e=1}^{e=l} t_e \int_{\Gamma_e} U^T \Phi Q d\Gamma_e . \quad (6)$$

555

556 A finite-element solution provides a minimum to functional (6) on the class of functions from a finite-
557 dimensional space with a basis $(\varphi_e)_{e=1}^{e=l}, \varphi_e = (\varphi_1^e, \varphi_2^e, \varphi_3^e)$ [1].

558 The necessary condition for the minimum of functional (6):

559
$$\sum_{\substack{e=1 \\ e=1,2,\dots,l}}^{e=l} \frac{\partial I^e}{\partial U} = \sum_{e=1}^{e=l} \int_{\Omega_e} t_e B^T D \cdot B \cdot U d\Omega_e - \sum_{e=1}^{e=l} \int_{\Gamma_e} t_e \Phi Q d\Gamma_e = 0, .$$

560 Therefore, we find the solution from the system of linear equations:

561

$$K_f \cdot U_f = F_f . \quad (7)$$

562

563 Here U_f is the global vector of nodal values:

564
$$U_f = (U^1, U^2, \dots, U^l)^T ,$$

565 K_f - a global stiffness matrix composed of element stiffness matrices (the so-called local stiffness
566 matrices) K^e :

$$K^e = \int_{\Omega_e} t_e B^T D B U d\Omega_e ,$$

F_f - global load vector, composed of load vectors of elements:

$$F_f^e = \int_{\Gamma_e} t_e \Phi^T Q d\Gamma_e .$$

Consider a boundary element with a distributed vertical load applied to it (Figure 3.3).

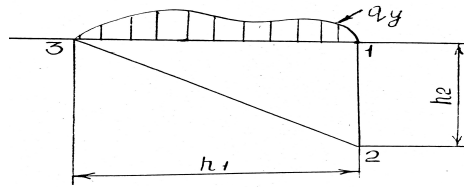


Figure 3.3 Scheme of load application to the boundary element

In the case of linear functions of the form, we have on the boundary:

$$\varphi_2 = 1 - \frac{s}{h_1} , \quad \varphi_3 = \frac{s}{h_1}$$

$$F_f^e = t_e \int_0^{h_1} \begin{pmatrix} 0 & 0 & 0 & \varphi_2 q_y & 0 & \varphi_3 q_y \end{pmatrix}^T dS . \quad (8)$$

Here are the specific values of the matrices and coefficients. Let's denote for convenience $\xi = \frac{h_1}{h_2}$.

The matrix B^e

Elements of the 1st type

$$B^{(1)} = \begin{bmatrix} 0 & 0 & -1/\xi & 0 & 1/\xi & 0 \\ 0 & \xi & 0 & -\xi & 0 & 0 \\ \xi & 0 & -\xi & -1/\xi & 0 & 1/\xi \end{bmatrix}$$

580

581

Elements of the 2nd type

582

$$B^{(2)} = \begin{bmatrix} 0 & 0 & 1/\xi & 0 & -1/\xi & 0 \\ 0 & -\xi & 0 & \xi & 0 & 0 \\ -xi & 0 & \xi & 1/\xi & 0 & -1/\xi \end{bmatrix}$$

583

584

Elements of the 3rd type

585

$$B^{(3)} = \begin{bmatrix} -1/\xi & 0 & 0 & 0 & 1/\xi & 0 \\ 0 & \xi & 0 & -\xi & 0 & 0 \\ \xi & -1/\xi & -xi & 0 & 0 & 1/\xi \end{bmatrix}$$

586

587

Elements of the 4th type

588

$$B^{(4)} = \begin{bmatrix} 1/\xi & 0 & 0 & 0 & -1/\xi & 0 \\ 0 & -\xi & 0 & \xi & 0 & 0 \\ -xi & 1/\xi & xi & 0 & 0 & -1/\xi \end{bmatrix}.$$

589

590

The Matrix K^e

591

We denote $d = \frac{1-\nu}{2}$

592

593

Elements of the 1st type

594

$$\frac{E}{2(1-\nu^2)} \begin{bmatrix} \xi d & 0 & -\xi d & -d & 0 & d \\ 0 & \xi & -\nu & -\xi & \nu & 0 \\ -\xi d & -\nu & 1/\xi + \xi d & \nu + d & -1/\xi & -d \end{bmatrix}$$

595

596

Elements of the 2nd type

$$\frac{E}{2(1-\nu^2)} \begin{bmatrix} -d & -\xi & \nu+d & \xi+d/\xi & -\nu & -d/\xi \\ 0 & \nu & -1/\xi & -\nu & 1/\xi & 0 \\ d & 0 & -d & -d/\xi & 0 & d/\xi \end{bmatrix}$$

Elements of the 3rd type

$$\frac{E}{2(1-\nu^2)} \begin{bmatrix} 1/\xi+\xi d & -\nu-d & -\xi d & \nu & -1/\xi & d \\ -\nu-d & \xi+d/\xi & d & -\xi & \nu & -d/\xi \\ -\xi d & d & \xi d & 0 & 0 & -d \end{bmatrix}$$

Elements of the 4th type

$$\frac{E}{2(1-\nu^2)} \begin{bmatrix} \nu & -\xi & 0 & \xi & -\nu & 0 \\ -1/\xi & \nu & 0 & -\nu & 1/\xi & 0 \\ d & -d/\xi & -d & 0 & 0 & d/\xi \end{bmatrix}.$$

The matrix K_f of the system (7) is composed of the stiffness matrices of the elements K^e in the following way. Suppose there are l -elements (Figure 3.1), we number all the vertices from left to right and from top to bottom. The matrix K_f has a dimension of $2 \cdot l \times 2 \cdot l$. Let's imagine it consisting of blocks (2x2). The dimension of such a matrix will be $l \times l$. Matrices of elements, as block ones, consisting of 2x2 submatrices, have a dimension of 3x3. Let the vertices of the elements belonging to the upper layer have numbers i and (or) $i+1$, and the vertices of the elements belonging to the lower layer have numbers j and (or) $j+1$. Then the following contribution to K_f will be made:

elements of the 1st type

$$K_f(j, j) = K_f(j, j) + KL(1, 1)$$

615 ($KL(1,1)$) - are the corresponding submatrices (2x2) of the matrix $K^{(1)}$)

$$\begin{aligned}
 &K_f(i, i) = K_f(i, i) + KL(2,2) \\
 &K_f(i+1, i+1) = K_f(i+1, i+1) + KL(3,3) \\
 616 &K_f(j, i) = K_f(j, i) + KL(1,2) \\
 &K_f(j, i+1) = K_f(j, i+1) + KL(1,3) \\
 &K_f(i+1, i) = K_f(i+1, i) + KL(3,2)
 \end{aligned}$$

617

618 elements of the 2nd type

$$\begin{aligned}
 &K_f(i+1, i+1) = K_f(i+1, i+1) + KL(1,1) \\
 &K_f(j+1, j+1) = K_f(j+1, j+1) + KL(2,2) \\
 619 &K_f(j, j) = K_f(j, j) + KL(3,3) \\
 &K_f(j+1, i+1) = K_f(j+1, i+1) + KL(2,1) \\
 &K_f(j+1, j) = K_f(j+1, j) + KL(2,3) \\
 &K_f(j, i+1) = K_f(j, i+1) + KL(3,1)
 \end{aligned}$$

620

621 elements of the 3rd type

$$\begin{aligned}
 &K_f(j, j) = K_f(j, j) + KL(1,1) \\
 &K_f(i, i) = K_f(i, i) + KL(2,2) \\
 622 &K_f(j+1, j+1) = K_f(j+1, j+1) + KL(3,3) \\
 &K_f(j, i) = K_f(j, i) + KL(1,2) \\
 &K_f(j+1, j) = K_f(j+1, j) + KL(3,1) \\
 &K_f(j+1, i) = K_f(j+1, i) + KL(3,2)
 \end{aligned}$$

623

624 elements of the 4th type

$$\begin{aligned}
 &K_f(i+1, i+1) = K_f(i+1, i+1) + KL(1,1) \\
 &K_f(j+1, j+1) = K_f(j+1, j+1) + KL(2,2) \\
 625 &K_f(i, i) = K_f(i, i) + KL(3,3) \\
 &K_f(i+1, i) = K_f(i+1, i) + KL(1,3) \\
 &K_f(j+1, i+1) = K_f(j+1, i+1) + KL(2,1) \\
 &K_f(j+1, i) = K_f(j+1, i) + KL(2,3)
 \end{aligned}$$

626

627 It is known from finite element theory [1] that the matrix K_f is symmetric and positive definite.

628 Therefore, the filling of elements lying only on the main diagonal and below is shown. Next, we

629 destroy the rows and columns of the matrix corresponding to the nodes (vertices) lying on the border of

630 the selected area (except for the zero horizontal).

631 In the case of modeling the impact of a load on a soil layer lying on a very weak foundation (eg

632 swamp), we do not impose restrictions on the lower boundary.

633 The contribution to the global load vector F_f - the right-hand side of system (7) is determined from

634 each element by formula (8). In this case, the node with the number t corresponds to the $(2t-1)$

635 and $2t$ lines of the vector F_f . Lines corresponding to border nodes are destroyed.

636 After finding the nodal displacements, the value of the stresses that are constant on the element is

637 determined by the formula (3). The values of the stresses at the nodes are found by averaging over

638 neighboring elements.

639 Stress matrix σ

640
$$\sigma = \begin{bmatrix} \sigma_x \\ \sigma_z \\ \tau_{xy} \end{bmatrix}.$$

641

642 Let's introduce the notation:

643
$$K_\sigma = \frac{E}{(1-\nu^2)h_1h_2}; \quad \alpha = \frac{1-\nu}{2};$$

644

645
$$u_{12} = u_1 - u_2, u_{13} = u_1 - u_3, u_{23} = u_2 - u_3, \\ v_{12} = v_1 - v_2, v_{13} = v_1 - v_3, v_{23} = v_2 - v_3.$$

646

647

Elements of the 1st type

648

$$\sigma = K_{\sigma} \begin{bmatrix} -h_2 u_{23} + v h_1 v_{12} \\ -v h_2 u_{23} + h_1 v_{12} \\ \alpha [h_1 u_{12} - h_2 v_{23}] \end{bmatrix}$$

649

650

Elements of the 2nd type

651

$$\sigma = K_{\sigma} \begin{bmatrix} h_2 u_{23} - v h_1 v_{12} \\ v h_2 u_{23} - h_1 v_{12} \\ -\alpha [h_1 u_{12} + h_2 v_{23}] \end{bmatrix}$$

652

653

Elements of the 3rd type

654

$$\sigma = K_{\sigma} \begin{bmatrix} -h_2 u_{13} + v h_1 v_{12} \\ -v h_2 u_{13} + h_1 v_{12} \\ \alpha [h_1 u_{12} - h_2 v_{13}] \end{bmatrix}$$

655

656

Elements of the 4th type

657

$$\sigma = K_{\sigma} \begin{bmatrix} h_2 u_{13} - v h_1 v_{12} \\ v h_2 u_{13} - h_1 v_{12} \\ -\alpha [h_1 u_{12} + h_2 v_{13}] \end{bmatrix} .$$

658

659 Further, according to the formulas of section (2), we determine the initial values of pressures, heads
 660 and stresses.

661 **4. Software implementation and calculation results**

662 **4.1 Main software modules**

663 MKESol – main module;

664 UnCode - contains subroutines for identifying the area of the partition;

665 SplinUnt - contains subroutines for constructing an interpolation cubic spline and for outputting spline

666 values at specified points;

667 GetSpline - the procedure for forming the global load vector (the right side of the linear algebraic

668 system of equations);

669 GetData - procedure for generating a global stiffness matrix;

670 LDL - contains routines for decomposition and solutions for strip matrices by the Cholesky method [7].

671 After the soil program has been processed, the values of the grid functions from the space V that

672 define the vertical and horizontal displacements are known. These values are recorded in the

673 Output.mke file;

674 MKEDrow - control module for presenting calculation results;

675 Sigma - contains programs for calculating mesh functions from a subspace U_1, \dots, U_s . The initial

676 data is the values of the mesh displacement functions contained in the Output.mke file;

677 FuncLoad - contains numerical integration routines for finding a solution to the first boundary value

678 problem in the case of an isotropic medium;

679 Anal - contains subroutines for graphical representation of a grid function in the form of function level

680 lines of two variables. This representation is performed by the LineLab (Nf, k) procedure. Here Nf is a

681 parameter defining the identifier code of the grid function; k is the number of level lines on the display

682 screen.

Nf	Level line
0	σ_x - steady-state stresses along the axis x , kg/cm^2
1	σ_z - steady-state stresses along the axis z , kg/cm^2
2	τ_{xz} - steady-state shear stresses along the axis x , kg/cm^2
3	σ_{xo} - initial stresses along the axis x , kg/cm^2
4	σ_{zo} - initial stresses along the axis z , kg/cm^2
5	P_o - initial pressures, kg/cm^2
6	V - vertical deformations, cm
7	Θ_{max} - the maximum angle of deviation of the full stress vector, $grad$
Encoding for solving the First Boundary Value Problem (FuncLoad module)	
10	σ_{xo} - initial stresses along the axis x , kg/cm^2
11	σ_{zo} - initial stresses along the axis z , kg/cm^2
12	P_o - initial pressures, kg/cm^2

Nf encoding table

4.2 Calculation results

686 The figures 4.1 - 4.4 show the results of calculating the zones of vertical stresses from the impact of the
 687 ML-56 machine for different types of tires:

688 33L-32F134;

689 33L-32F134M - with reduced pressure;

690 71x47-25; 79x59-26} ultra wide-profile.

691 Movement on loamy soil is simulated. The soil is presented in two layers: a thin layer of 30 cm on a

692 denser base. The relative humidity of the soil is 80%. The characteristics of the soil are presented in the
693 table 4.1.

	Deformation modulus $E, \text{ kg/cm}^2$	Poisson's ratio ν	Internal grip $C_o, \text{ kg/cm}^2$	Internal friction angle $\varphi_o, \text{ grad.}$
Upper layer	100	0,3	0,21	15
Bottom layer	370	0,3	0,60	18

Table 4.1 Soil characteristics

694 An intensive increase in rutting can be expected during trips by the machine with 33L-32F134 tires as a
695 result of vertical deformation in the soil and lateral uplift caused by the movement of destroyed soil
696 into zones with zero and negative (i.e. tensile) vertical stresses. This is the manifestation of the flat
697 phenomena of the mathematical model.

698

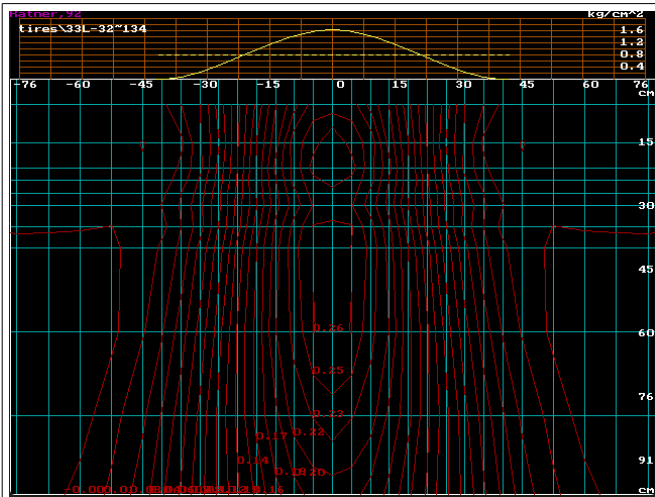


Figure 4.1 Distribution of initial stresses
 $(\sigma_{z0}, \text{ kg/cm}^2)$. Tires 33L-32FI34

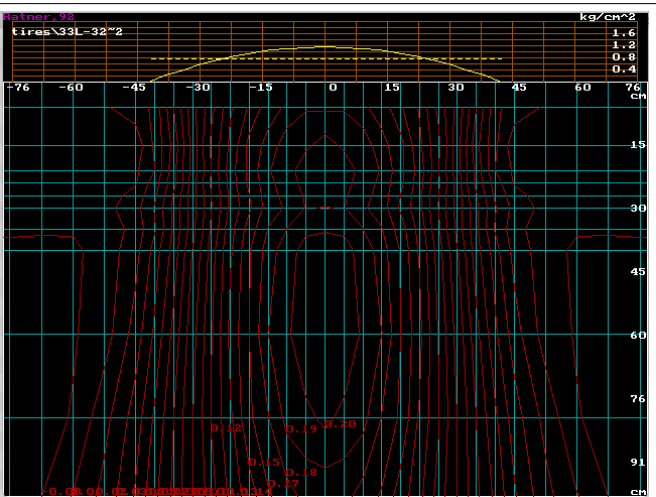


Figure 4.2 Distribution of initial stresses
 $(\sigma_{z0}, \text{ kg/cm}^2)$. Tires 33L-32FI34 M

Comparing the figures 4.1 and 4.2, we can note the absence of soil zones with a destroyed structure

(figure 4.2) in the case of using the 33L-32F134 M tire with an internal air pressure of 0.8 kg / cm ^ 2. This is due to a change in the shape of the loading diagram with a decrease in the internal air pressure from 1.4 to 0.8 kg / cm ^ 2.

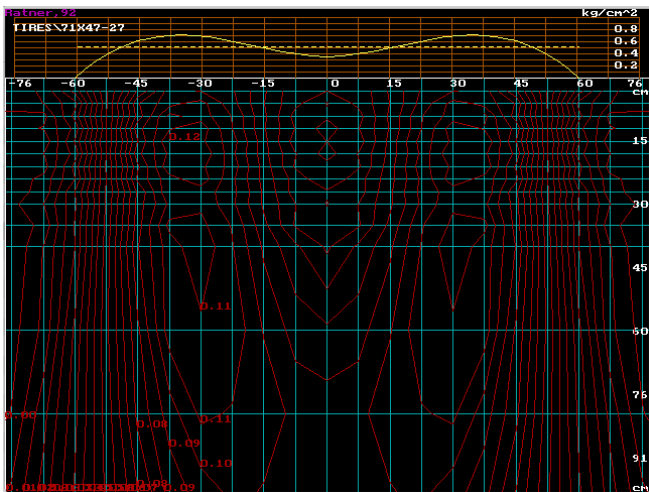


Figure 4.3 Distribution of initial stresses (σ_{z_0} , kg/cm²) . Tires 71x47-25

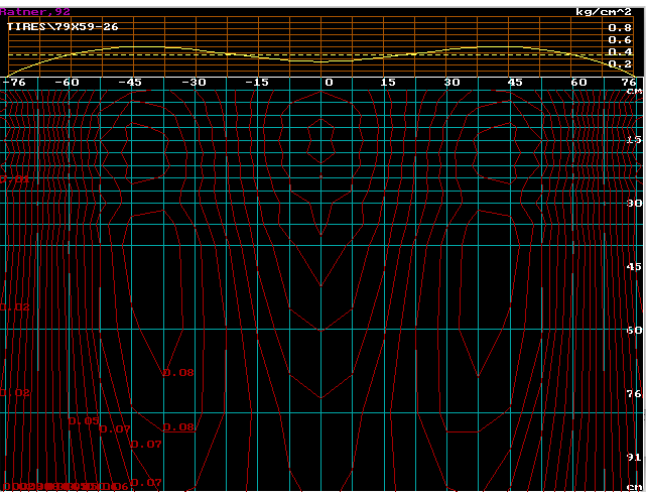


Figure 4.4 Distribution of initial stresses (σ_{z_0} , kg/cm²) . Tires 79x59-26

A significant reduction in the stress state of the soil is observed with the use of ultra-wide-profile tires.

5. Experimental data

The figures 5.1 – 5.4 show the calculated zones of vertical stresses from the impact of the TT-4M tractor with a highly elastic and serial track. The soil is homogeneous (in modulus of deformation), therefore, an analytical solution to the first boundary value problem is presented. The characteristics of the soil are presented in table 5.1. Available experimental data [8] (mean values of pressure sensors over time series) are presented in Table 5.2.

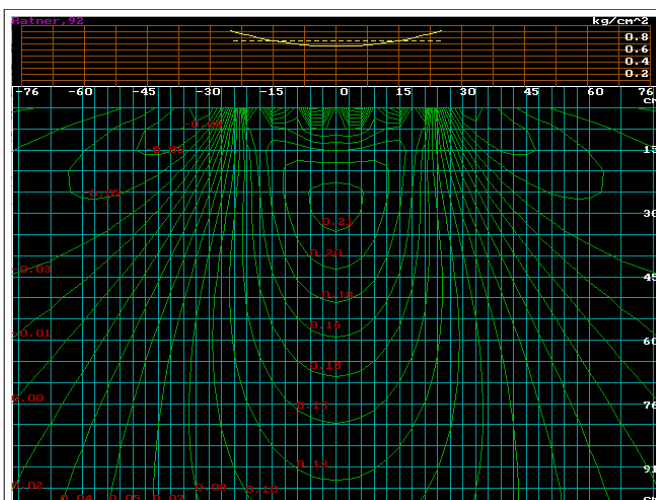


Figure 5.1 Distribution of initial stresses σ_{z0} , kg/cm^2 in a homogeneous medium. Serial track.

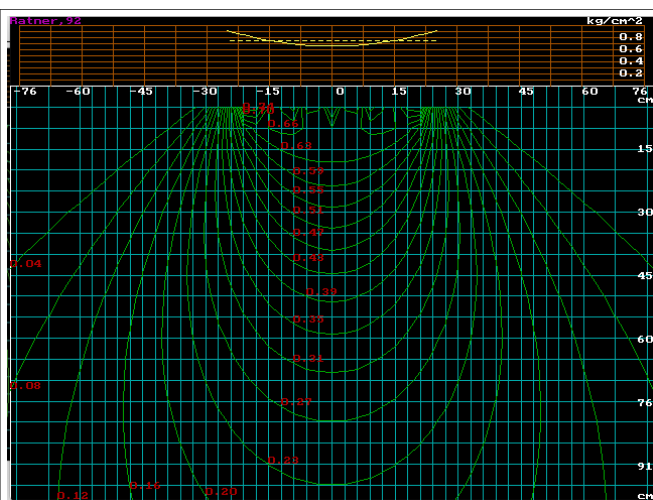


Figure 5.2 Distribution of steady-state stresses σ_z , kg/cm^2 in a homogeneous medium. Serial track.

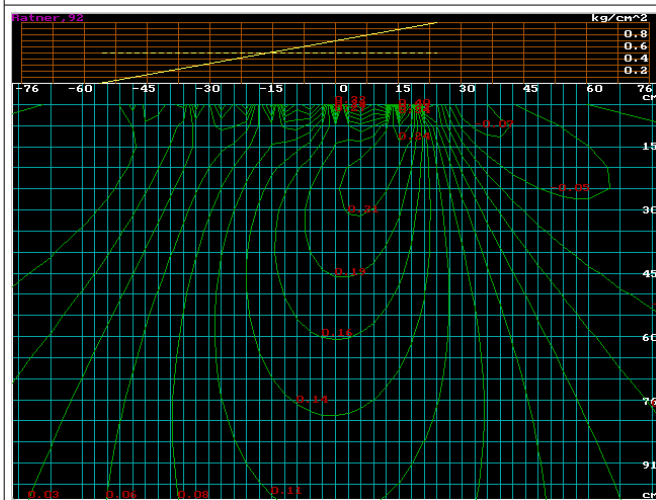


Figure 5.3 Distribution of initial stresses σ_{z0} , kg/cm^2 in a homogeneous medium. Highly elastic track.

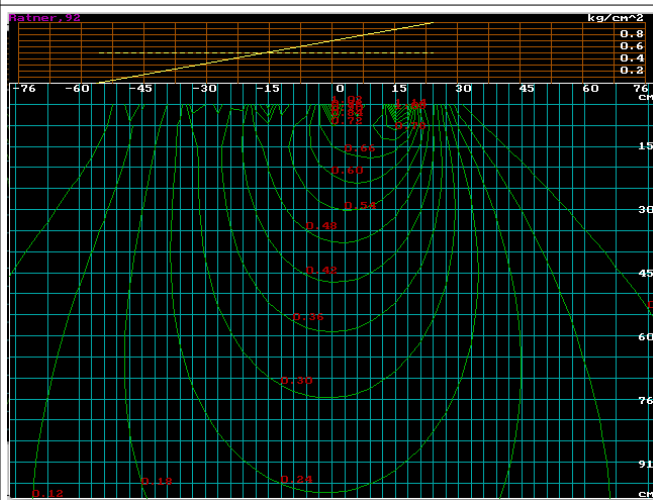


Figure 5.4 Distribution of steady-state stresses σ_z , kg/cm^2 in a homogeneous medium. Highly elastic track.

Sampling depth, cm	The number of strikes by the a striker	Soil deformation modulus for a striker, MPA	Density of wet soil g/cm^3	Density of the soil skeleton g/cm^3
20	3.33	5.0	2.04	1.7
40	4.0	6.0	2.02	1.68
60	2.75	4.12	2.11	1.74

Table 5.1 Physical and mechanical indicators of soils and grounds on measured plots

708

Distance from the center of the treadmill to the pressure sensors, cm			
	-25	0	25
Serial track. Gross weight of the tractor 21250 kg			
Top row	0.090	0.384	...
+ 20 cm	0.196	0.333	0.357
+ 40 cm	...	0.231	...
Highly elastic track. Gross weight of the tractor 23900 kg			
Top row	0.060	...	1.538
+ 20 cm	0.190	0.282	0.289
+ 40 cm	...	0.189	...

Table 5.2 Average values of pressures, kg/cm^2

709 It can be seen from Table 5.2 that the general view of the calculated distribution functions of vertical
710 stresses for both types of tracks is in good agreement with the experimental data. The experimental
711 values of stresses are greater than the initial calculated values, but less than the steady-state values of
712 stresses. This can be explained by the following factors:

713 a) The initial distance from the top layer of the sensors (20 cm) decreased as a result of soil

714 deformation.

715 b) The values of pressures averaged over the time series are taken as experimental data, i.e. pressure
716 from the load, which acts for some time, and the initial stresses from the instantly applied load are
717 taken as the calculated ones, the value of which is averaged over the reference area of the track.
718 c) Pressure sensors perceive the load, the components of which are the load from water pressure and
719 the load from vertical stresses in the soil skeleton, and we calculate only vertical stresses in the
720 skeleton.

721

722 ***Conclusion***

723 The presented mathematical model, together with its software implementation, makes it possible to
724 assess the degree of influence of the tire of a forest wheeled tractor on the waterlogged forest soil,
725 depending on the design parameters of the tire and the vertical loads that fall on it.

726 The adequacy of the mathematical model is confirmed by the conducted experimental studies, as well
727 as by numerous test results of forest wheeled tractors.

728 The model is developed based on the theory of soil mechanics. The plane problem of compaction of
729 water-saturated anisotropic (in the general case) soil is considered. It was shown that with an
730 instantaneous application of a vertical load, the initial distribution of stress and water pressure in the
731 soil are expressed through their values in a state of complete stabilization. Therefore, it is
732 conventionally assumed that the magnitude of the load does not change before the onset of this state,
733 causing linear (relative to the load) deformations of the soil.

734 Thus, first, a plane problem of different modulus of the theory of a linearly deformable medium is
735 solved. This problem is described by a system of partial differential equations (equations 7-9 of section

736 1). The solution is found by the finite element method with respect to displacements. Then, the steady-
737 state and initial values of the stresses are determined, as well as the values of the maximum deviation
738 of the total stress vector - θ_{max} .

739 In the case of an isotropic medium, the initial heads function (H_o) satisfies the Laplace equation:

740 $\Delta H_o = 0$. The first boundary value problem is posed and solved. Analytical expressions are
741 obtained for the initial values of water heads, pressure and stresses. With their help, one can select the
742 optimal triangulation of the region for a given loading diagram and check the finite element solution.

743 The initial data for this mathematical model are the layer-by-layer values of the deformation modulus,
744 Poisson's ratio, adhesion coefficient C_o , and angle of internal friction φ_o . Condition: $\theta_{max} = \infty$
745 means that the soil mass is in a state of ultimate plastic equilibrium.

746 The calculation results are presented as level lines of the function of two variables. The general view of
747 the vertical stress function is in good agreement with the available experimental data.

748 It was found that the form of the transverse loading diagram has a significant effect on the degree of the
749 stress state of the soil. At the same average contact pressures, the parabolic shape of the loading
750 diagram, which is characteristic of tires with reduced internal air pressure, has the smallest effect on the
751 soil.

752 The method can serve as the basis for predicting the degree of soil compaction and the intensity of
753 rutting, as well as the environmental consequences of the operation of forest machines.

754 ***Acknowledgement***

755 I am sincerely grateful to Mr. Philip Rodriguez for his help in preparing the text.

Computer Code Availability

756
757 Name of code: soil-models;
758 developer: Dr. Igor Ratnere, Lawrence Berkeley National Laboratory
759 1 Cyclotron Road, M/S 91R0183, Berkeley, CA 94720, 510-495-8373 (Office), iratnere@lbl.gov
760 year first available: 1992
761 hardware required: Mac (Mac OS) or PC (Windows)
762 software required: DosBox, Turbo Pascal [<https://gist.github.com/nvgrw/da00b5d3ac96b9c45c80>]
763 program language: Turbo Pascal
764 program size: 408 KB
765 <https://github.com/igorratn/soil-models.git>

References

- 768
769 1. Ciarlet P.G. 1980. The finite element method for elliptic problems. Mir, M., 512 pp. [in Russian].
770 2. Gersevanov N.M. 1948. Research in the field of soil dynamics, mechanics and applied mathematics.
771 Stroyvoenmorizdat, M., 376 pp. [in Russian].
772 3. Florin V.A. 1954. Fundamentals of Soil Mechanics, Vol.1. Gosstroyizdat, M., 358 pp. [in Russian].
773 4. Florin V.A. 1961. Fundamentals of Soil Mechanics, Vol.2. Gosstroyizdat, M., 544 pp. [in Russian].
774 5. Nikiforov A.F. 1983. Methods of Mathematical Physics. Ed. Moscow State University, M., 224 pp.
775 [in Russian].
776 6. Pokrovsky G.I. 1941. Friction and traction in soils. Stroyizdat, M., 120 pp. [in Russian].

- 777 7. Reinsch C. , Wilkinson J.H. 1976. Algorithms reference book in the Algol language. Linear algebra.
778 Mechanical engineering, M., 392 pp. [in Russian].
- 779 8. Ratner I.S. 1993. Determination of traction reference indicators of a wheeled forestry tractor and
780 assessment of soil condition parameters. Dissertation for the degree of candidate of technical sciences.
781 Khimki, 215 pp. [in Russian].
- 782 9. Terzagi K. 1961. Theory of soil mechanics, Stroyizdat, M., 508 pp. [in Russian].
- 783 10. S.P. Timoshenko, J.N. Goodier, 1975. Theory of elasticity. Science, M., 576 pp. [in Russian].